An Iterative Algorithm with Joint Sparsity Constraints for Magnetic Tomography

Francesca Pitolli, Gabriella Bretti *

Dip. Me.Mo.Mat., Università di Roma "La Sapienza"

Via A. Scarpa 10, 00161 Roma, Italy

Abstract

Magnetic tomography is an ill-posed and ill-conditioned inverse problem since, in general, the solution is non-unique and the measured magnetic field is affected by high noise.

We use a joint sparsity constraint to regularize the magnetic inverse problem. This leads to a minimization problem whose solution can be approximated by an iterative thresholded Landweber algorithm. The algorithm is proved to be convergent and an error estimate is also given.

Numerical tests on a bidimensional problem show that our algorithm outperforms Tikhonov regularization when the measurements are distorted by high noise.

Keywords: Magnetic tomography, Inverse problem, Sparsity constraint, Iterative thresholding, Multiscale basis.

1 Introduction

The magnetic tomography aims at spatially resolve an unknown vector-valued current distribution from its magnetic field measured in the outer space.

* *E-mail address:* {pitolli,bretti}@dmmm.uniroma1.it

Magnetic tomography has applications in many fields, i.e. geophysics, archaeological investigations, medicine, microelectronic, nondestructive testing. In particular, we focus our interest on magnetoencephalography (MEG) and nondestructive evaluation (NDE) of structures. MEG aims to identify the regions of the brain where the neuronal activity is located by detecting the regions where bioelectric currents flows, while NDE aims to localize cracks and corrosion damage which appear as perturbations of the current distribution within a given material [19]. In both cases an image of the current distribution within the object under investigation has to be reconstructed in a noninvasive way, i.e. by the magnetic field measured by sensors located in the outer space.

Since the magnetic field decreases very fast as the distance between the current source and the sensor position increases, the measured magnetic field can be very weak and affected by high noise. Usually, the measurements are performed by very sophisticated instrumentations based on Superconducting QUantum Interference Device (SQUID) magnetometers that can measure magnetic fields generated by deep currents [19]. Even if SQUID magnetometers are able to measure very weak field, nevertheless the measurements are distorted by high noise and a sophisticated data analysis is needed.

In magnetic tomography, the measurements do not give an immediate current image. In order to produce a current image, first of all, we need a model to relate the current distribution and the external magnetic field; then, we have to solve an inverse problem. In literature, this problem is known as magnetic inverse problem, and, in general, do not have a unique solution, so that regularization techniques are needed [2], [14], [17].

The well-known Tikhonov regularization, which uses a quadratic constraint, gives good results when the quantities under observation are equally distributed in time or space [1], [8]. Actually, in MEG and NDE applications the regions where the currents flow are usually small. This means that the current distribution we want to reconstruct is spatially inhomogeneous and can be represented as a sum of weighted basic currents where only few terms are relevant. To reconstruct quantities with sparse patterns a regularization technique based on *sparsity constraints* can be used; this leads to a thresholded Landweber algorithm which is able to approximate the solution of a linear inverse problem in an efficient way [5].

Our aim is to solve the magnetic inverse problem by using a joint sparsity constraint as a regularization technique. Joint sparsity has been introduced in [11] in order to deal with problems where the quantities to reconstruct are

vector-valued functions. The solution of the MEG inverse problem with joint sparsity constraints has been addressed in [10]. Here, we focus our attention on NDE applications of the magnetic tomography. The forward and inverse magnetic NDE problems are addressed in Section 2. Then, in Section 3 we introduce a joint sparsity constraint as a regularization term. An efficient algorithm to solve the problem is given in Section 4. Finally, some numerical tests on a bidimensional problem are shown in Section 5.

2 The Forward and Inverse Magnetic NDE Problems

NDE problems can be modeled by the Maxwell's equations for a polarizable and magnetizable macroscopic media [2]. In particular, the electric field $\vec{\mathbf{E}}$ and the magnetic field $\vec{\mathbf{B}}$ can be described by the quasi-static Maxwell's equations

$$\begin{aligned} \operatorname{curl} \vec{\mathbf{E}} &= 0, \\ \operatorname{curl} \vec{\mathbf{B}} &= \mu_0 \, \vec{\mathbf{J}}, \\ \operatorname{div} \vec{\mathbf{B}} &= 0, \end{aligned} \tag{2.1}$$

where $\vec{\mathbf{J}}$ is the current density in the medium and μ_0 is the magnetic permeability of the vacuum.

Due to the conservation of the charge, the current density satisfies

$$\operatorname{div} \vec{\mathbf{J}} = 0. \tag{2.2}$$

In the following we assume that the volume V_0 where the current flows is a slab of thickness d, with the surfaces of the slab at $z = \pm d/2$. The magnetometers are located on an horizontal plane $\mathbf{\Pi}$ at $z = \pi$, with

$$\pi := \operatorname{dist}(\partial V_0, \mathbf{\Pi}) > \frac{d}{2}, \tag{2.3}$$

and they measure only B_z, the component of the magnetic field along $\vec{\mathbf{e}}_z$, the normal w.r.t. to $\mathbf{\Pi}$ (see Fig. 1).

From the quasi-static Maxwell's equations it follows that the magnetic field $\vec{\mathbf{B}}$ generated by the current $\vec{\mathbf{J}}$ obeys the *Biot-Savart law* [2], [13], [17]

$$\vec{\mathbf{B}}(\vec{\mathbf{r}}) = \frac{\mu_0}{4\pi} \int_{V_0} \vec{\mathbf{J}}(\vec{\mathbf{r}}\,') \times \frac{\vec{\mathbf{r}} - \vec{\mathbf{r}}\,'}{|\vec{\mathbf{r}} - \vec{\mathbf{r}}\,'|^3} \, d\vec{\mathbf{r}}\,'. \tag{2.4}$$

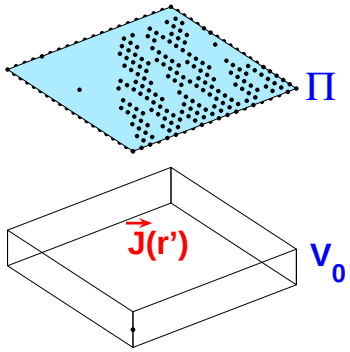

Figure 1: The NDE problem setting.

Here, $\vec{\mathbf{v}}\times\vec{\mathbf{w}}$ is the usual cross product of vectors in $\mathbb{R}^3$ and $|\vec{\mathbf{v}}|$ is the Euclidean norm of the vector $\vec{\mathbf{v}}$.
For $B_z(\vec{\mathbf{r}})$ we have

$$\begin{aligned} B_z(\vec{\mathbf{r}}) &= \frac{\mu_0}{4\pi}\int_{V_0}\frac{\vec{\mathbf{J}}(\vec{\mathbf{r}}\,')\times(\vec{\mathbf{r}}-\vec{\mathbf{r}}\,')}{|\vec{\mathbf{r}}-\vec{\mathbf{r}}\,'|^3}\cdot\vec{\mathbf{e}}_z(\vec{\mathbf{r}})\,d\vec{\mathbf{r}}\,' = \\ &= \frac{\mu_0}{4\pi}\int_{V_0}\frac{\vec{\mathbf{e}}_z(\vec{\mathbf{r}})\times(\vec{\mathbf{r}}\,'-\vec{\mathbf{r}})}{|\vec{\mathbf{r}}\,'-\vec{\mathbf{r}}|^3}\cdot\vec{\mathbf{J}}(\vec{\mathbf{r}}\,')\,d\vec{\mathbf{r}}\,', \qquad \vec{\mathbf{r}}\in\mathbf{\Pi}, \end{aligned} \tag{2.5}$$

where the equality in the second line follows from the relation $\vec{\mathbf{v}}\times\vec{\mathbf{w}}\cdot\vec{\mathbf{z}} = -\vec{\mathbf{z}}\times\vec{\mathbf{w}}\cdot\vec{\mathbf{v}}$, holding for any $\vec{\mathbf{v}},\vec{\mathbf{w}},\vec{\mathbf{z}}\in\mathbb{R}^3$.

Now, let $\vec{\mathbf{q}}_l\in\mathbf{\Pi}$, $l=1,\ldots,N$, be the locations of the magnetometers and let

$$\mathcal{B}(\vec{\mathbf{J}},\vec{\mathbf{q}}_l) := B_z(\vec{\mathbf{q}}_l) = \frac{\mu_0}{4\pi}\int_{V_0}\frac{\vec{\mathbf{e}}_z(\vec{\mathbf{q}}_l)\times(\vec{\mathbf{r}}\,'-\vec{\mathbf{q}}_l)}{|\vec{\mathbf{r}}\,'-\vec{\mathbf{q}}_l|^3}\cdot\vec{\mathbf{J}}(\vec{\mathbf{r}}\,')\,d\vec{\mathbf{r}}\,' \tag{2.6}$$

be the normal component of the magnetic field evaluated in $\vec{\mathbf{q}}_l$.

Observe that the magnetic field at different values of z are related by inward continuation, so that we cannot obtain additional information by measuring the magnetic field on planes at different heights. By the way, since

curl $\vec{\mathbf{B}} = 0$ and div $\vec{\mathbf{B}} = 0$ in the outer space, information on the z-component of the magnetic field is sufficient to determine the whole magnetic field [15].

The magnetic NDE inverse problem aims at reconstruct the current distribution $\vec{\mathbf{J}}$ starting from the normal component of the magnetic field, measured in $\vec{\mathbf{q}}_l$, $l = 1, \ldots, N$.

In order to identify the current sources from the measurements $\mathbf{M} = \{m_1, \ldots, m_N\}$ we have to minimize the discrepancy

$$\Delta(\vec{\mathbf{J}}) := \left\| \mathbf{G}(\vec{\mathbf{J}}) - \mathbf{M} \right\|^2_{\mathbb{R}^N}, \tag{2.7}$$

where

$$\mathbf{G}(\vec{\mathbf{J}}) = \{\mathcal{B}(\vec{\mathbf{J}}, \vec{\mathbf{q}}_1), ..., \mathcal{B}(\vec{\mathbf{J}}, \vec{\mathbf{q}}_N)\}. \tag{2.8}$$

Unfortunately, this is a strongly ill-posed problem since there exist silent currents that do not produce magnetic field in the outer space, so that non unique solutions can be expected. Moreover, the intensity of the magnetic field decreases fast as the height of the plane $\mathbf{\Pi}$ increases, so that the measured magnetic field can be very low and affected by high noise. For these reasons the minimization of the discrepancy might not be feasible and some regularization technique is required. This will be the subject of the following section.

3 The Magnetic NDE Inverse Problem with Sparsity Constraints

We assume that the current distribution we want to reconstruct is spatially inhomogeneous and can be represented as a sum of weighted basic currents belonging to a dictionary, such that only few terms in the sum are relevant. More formally, we assume that [6]

Definition 1. *The current density* $\vec{\mathbf{J}} = (J_1, J_2, J_3) \in L_2(V_0; \mathbb{R}^3)$ *is* sparsely *represented by a suitable dictionary* $\mathcal{D} := \{\psi_\lambda\}_{\lambda \in \mathbf{\Lambda}}$, *i.e.*

$$J_\ell \approx \sum_{\lambda \in \mathbf{\Lambda}_S} j^\ell_\lambda \, \psi_\lambda \,, \qquad j^\ell_\lambda = \langle J_\ell, \psi_\lambda \rangle \,, \qquad \ell = 1, 2, 3, \tag{3.1}$$

where $\mathbf{\Lambda}_S \subset \mathbf{\Lambda}$ *is the set of the* few *significant coefficients* j^ℓ_λ.

As a dictionary we choose a stable multiscale basis $\{\psi_\lambda\}_{\lambda\in\mathbf{\Lambda}} \in L_2(V_0,\mathbb{R})$, i.e. a function basis satisfying the inequality

$$C_1\|f\|^2_{L_2(V_0)} \le \sum_{\lambda\in\mathbf{\Lambda}} |\langle f,\psi_\lambda\rangle|^2 \le C_2\|f\|^2_{L_2(V_0)}, \quad \lambda\in\mathbf{\Lambda}, \tag{3.2}$$

for all $f \in L_2(V_0)$. Suitable dictionaries are, for instance, wavelets [4] or frames [3].

In order to enforce sparsity on the solution of the magnetic NDE inverse problem we use a sparsity constraint as follows.

Given a set of magnetic field measurements $\mathbf{M}$*, determine a configuration of the current density* $\vec{\mathbf{J}}$ *that minimizes the functional*

$$\mathcal{J}_{\mathbf{\Psi}}(\vec{\mathbf{J}}) := \mathbf{\Delta}(\vec{\mathbf{J}}) + \mathbf{\Psi}_{\mathcal{D}}(\vec{\mathbf{J}}), \tag{3.3}$$

where $\mathcal{D}$ *is a dictionary chosen in order the solution of the minimum problem is sparsely represented, and* $\mathbf{\Psi}_{\mathcal{D}}$ *is a suitable* sparsity measure *w.r.t.* $\mathcal{D}$*.*

A sparsity measure for the regularization of linear ill-posed problems when the quantity to reconstruct is a scalar function f, has been introduced in [5]. In this case

$$\mathbf{\Psi}_{\mathcal{D}}(f) := \sum_{\lambda\in\mathbf{\Lambda}} v_\lambda \left|\langle f,\psi_\lambda\rangle\right|^p, \qquad p\ge 1, \tag{3.4}$$

where $\{v_\lambda\}_{\lambda\in\Lambda}$ are nonnegative weights. The solution of the related minimization problem leads to an iterative thresholded Landweber algorithm.

Since in our problem the current $\vec{\mathbf{J}}$ is a vector-valued function, a suitable sparsity measure is the joint sparsity introduced in [11].

Definition 2. *Let* $\vec{\mathbf{F}} = (F_1, F_2, F_3)$ *be a vector-valued function in* $L_2(V_0,\mathbb{R}^3)$*, and let* $\{\psi_\lambda\}_{\lambda\in\mathbf{\Lambda}}$ *be a dictionary. Let us denote by*

$$\vec{\mathbf{f}}_\lambda = (f^1_\lambda, f^2_\lambda, f^3_\lambda) \quad \textit{with} \quad f^\ell_\lambda = \langle F_\ell,\psi_\lambda\rangle \tag{3.5}$$

the decomposition coefficients of $\vec{\mathbf{F}}$ *and by* $\|\vec{\mathbf{f}}_\lambda\|_p$ *the usual p-norm for vectors. Given the positive sequences* $\{\theta_\lambda\}_{\lambda\in\mathbf{\Lambda}}$*,* $\{\rho_\lambda\}_{\lambda\in\mathbf{\Lambda}}$*,* $\{\omega_\lambda\}_{\lambda\in\mathbf{\Lambda}}$*, we define the joint sparsity measure as the functional*

$$\mathbf{\Psi}^{(p)}_{\mathcal{D}}(\vec{\mathbf{F}},v) := \sum_{\lambda\in\mathbf{\Lambda}} v_\lambda \|\vec{\mathbf{f}}_\lambda\|_p + \sum_{\lambda\in\mathbf{\Lambda}} \omega_\lambda \|\vec{\mathbf{f}}_\lambda\|_2^2 + \sum_{\lambda\in\mathbf{\Lambda}} \theta_\lambda(\rho_\lambda - v_\lambda)^2, \quad p\ge 1. \tag{3.6}$$

By using the decomposition (3.1), the discrepancy (2.7) can be written as

$$\Delta(\vec{\mathbf{j}}) = \left\| T\,\vec{\mathbf{j}} - \mathbf{M} \right\|^2_{\mathbb{R}^N}, \tag{3.7}$$

where $\vec{\mathbf{j}} := \{j^\ell_\lambda\}_{\lambda\in\Lambda,\ell=1,2,3}$ and the operator $T : \ell_2(\Lambda,\mathbb{R}^3) \to \mathbb{R}^N$ has entries given by

$$(T\,\vec{\mathbf{j}})_l \;=\; \sum_{\ell=1}^{3}\sum_{\lambda\in\mathbf{\Lambda}} j^\ell_\lambda\,\frac{\mu_0}{4\pi}\int_{V_0}\left(\frac{\vec{\mathbf{e}}_z(\vec{\mathbf{q}}_l)\times(\vec{\mathbf{r}}\,'-\vec{\mathbf{q}}_l)}{|\vec{\mathbf{r}}\,'-\vec{\mathbf{q}}_l|^3}\right)_\ell \psi_\lambda(\vec{\mathbf{r}}\,')\,d\vec{\mathbf{r}}\,'. \tag{3.8}$$

Thus, the magnetic NDE inverse problem with the joint sparsity constraint consists in minimizing the functional

$$\begin{aligned}\mathcal{J}^{(p)}_{\theta,\omega,\rho}(\vec{\mathbf{j}},v) &= \left\| T\vec{\mathbf{j}} - \mathbf{M} \right\|^2_{\mathbb{R}^N} + \mathbf{\Psi}_{\mathcal{D}}(\vec{\mathbf{j}},v) = \\ &= \sum_{l=1}^{N}\left|(T\vec{\mathbf{j}})_l - m_l\right|^2 + \sum_{\lambda\in\mathbf{\Lambda}} v_\lambda\,\|\vec{\mathbf{j}}_\lambda\|_p + \sum_{\lambda\in\mathbf{\Lambda}}\omega_\lambda\|\vec{\mathbf{j}}_\lambda\|_2^2 + \sum_{\lambda\in\mathbf{\Lambda}}\theta_\lambda(\rho_\lambda - v_\lambda)^2\end{aligned} \tag{3.9}$$

jointly with respect to both $\vec{\mathbf{j}}$ and v, restricted to $v_\lambda \geq 0$.

The minimization of the functional (3.9) promotes that all entries of the vector $\vec{\mathbf{j}}_\lambda$ have the *same sparsity* pattern. Note that v serves as an indicator of large values of $\|\vec{\mathbf{j}}_\lambda\|_p$ and $0 \leq v_\lambda \leq \rho_\lambda$, $\lambda \in \mathbf{\Lambda}$, at the minimum. The quadratic term $\displaystyle\sum_{\lambda\in\mathbf{\Lambda}}\omega_\lambda\|\vec{\mathbf{j}}_\lambda\|_2^2$ makes the overall functional convex, depending on a suitable choice of the sequence $\{\omega_\lambda\}_{\lambda\in\mathbf{\Lambda}}$.

We remark that when $\theta_\lambda = 0$ and $\omega_\lambda = \alpha$ (a fixed constant) for all $\lambda \in \Lambda$, we obtain the usual Tikhonov regularization since $\{v_\lambda\}_{\lambda\in\Lambda} = 0$ in this case.

The convexity conditions for the functional $\mathcal{J}^{(p)}_{\theta,\rho,\omega}$ depend on the values of the parameters $\{\theta_\lambda\}_{\lambda\in\mathbf{\Lambda}}$, $\{\rho_\lambda\}_{\lambda\in\mathbf{\Lambda}}$, $\{\omega_\lambda\}_{\lambda\in\mathbf{\Lambda}}$. Details can be found in [11]. In particular, we recall that for $p = 1, 2, \infty$, $\mathcal{J}^{(p)}_{\theta,\rho,\omega}$ is convex if

$$(s_{\min} + \omega_\lambda)\,\theta_\lambda \geq \frac{\kappa_p}{4} = \begin{cases} \frac{3}{4} & \text{if} \quad p = 1, \\ \\ \frac{1}{4} & \text{if} \quad p = 2, \infty, \end{cases} \tag{3.10}$$

where $s_{\min}$ is the minimum of the spectrum of T^*T. In case of strict inequality, $\mathcal{J}^{(p)}_{\theta,\rho,\omega}$ is strictly convex.

4 The Minimizing Algorithm

The minimizer $\vec{\mathbf{j}}^*$ of the functional $\mathcal{J}^{(p)}_{\theta,\rho,\omega}$ can be approximated by the following thresholded Landweber algorithm, deduced from [12].

Algorithm 1.

$$\begin{cases} \text{Let } \gamma \text{ be a suitable relaxation parameter} \\ \\ \text{Choose an arbitrary} \quad \vec{\mathbf{j}}^{(0)} \in \ell_2(\mathbf{\Lambda};\mathbb{R}^3) \\ \\ \text{For} \quad 0 \le k \le K \quad \text{do} \quad \vec{\mathbf{j}}^{(k+1)} = H^{(p)}_{\theta,\rho,\omega}\left(\vec{\mathbf{j}}^{(k)} + \gamma\, T^*(M - T)\,\vec{\mathbf{j}}^{(k)}\right) \\ \\ \text{Compute} \quad v_\lambda^{(K+1)} = \begin{cases} \rho_\lambda - \frac{1}{2\theta_\lambda}\|\vec{\mathbf{j}}_\lambda^{(K+1)}\|_p & \text{if } \|\vec{\mathbf{j}}_\lambda^{(K+1)}\|_p < 2\theta_\lambda\rho_\lambda \\ 0 & \text{otherwise} \end{cases} \qquad \lambda \in \mathbf{\Lambda} \end{cases}$$

(usually, the values $\{v_\lambda^{(K)}\}_{\lambda\in\mathbf{\Lambda}}$ are not needed).

The operator $H^{(p)}_{\theta,\rho,\omega}$ is a thresholding operator acting on a vector-valued function $\vec{\mathbf{f}} \in \ell_2(\mathbf{\Lambda};\mathbb{R}^3)$ as

$$\left(H^{(p)}_{\theta,\rho,\omega}(\vec{\mathbf{f}})\right)_\lambda := (1+\omega_\lambda)^{-1} h^{(p)}_{\theta_\lambda(1+\omega_\lambda),\rho_\lambda}(\vec{\mathbf{f}}_\lambda), \quad \lambda \in \mathbf{\Lambda}. \tag{4.1}$$

The explicit expression of $h^{(p)}_{\theta,\rho}$ can be found in [11], but an efficient algorithm for the evaluation of $h^{(p)}_{\theta,\rho}(\vec{\mathbf{f}}_\lambda)$ is given in [12].

Algorithm 2.

$$\begin{cases} \text{Choose a positive sequence} \quad v^{(0)} \\ \\ \text{Let } \vec{\mathbf{f}}^{(0)} = \vec{\mathbf{f}}_\lambda \\ \\ \text{For} \quad 0 \le k \le K \quad \text{do} \\ \\ \qquad \vec{\mathbf{f}}^{(k+1)} = S^{(p)}_{v^{(k)}} \left(\vec{\mathbf{f}}^{(k)} \right) \\ \\ \qquad v_\lambda^{(k+1)} = \begin{cases} \rho_\lambda - \frac{1}{2\theta_\lambda} \|\vec{\mathbf{f}}^{(k+1)}\|_p & \text{if } \|\vec{\mathbf{f}}^{(k+1)}\|_p < 2\theta_\lambda \rho_\lambda \\ 0 & \text{otherwise} \end{cases} \qquad \lambda \in \mathbf{\Lambda} \\ \\ \text{Approximate} \quad h^{(p)}_{\theta,\rho}(\vec{\mathbf{f}}_\lambda) \approx \vec{\mathbf{f}}^{(K+1)} \end{cases}$$

The operator $S_v^{(p)}$ is itself a thresholding operator whose explicit expression for $p = 1, 2$ is (cf. [11]):

$$\left(S_v^{(1)}(\vec{\mathbf{f}})\right)_\ell = s_v^{(1)}(f_\ell) = \begin{cases} \operatorname{sign}(f_\ell) \left(|f_\ell| - \frac{v}{2} \right) & \text{if} \quad |f_\ell| > \frac{v}{2}, \\ \\ 0 & \text{otherwise}, \end{cases} \tag{4.2}$$

$$S_v^{(2)}(\vec{\mathbf{f}}) = \begin{cases} \frac{\|\vec{\mathbf{f}}\|_2 - v/2}{\|\vec{\mathbf{f}}\|_2} \, \vec{\mathbf{f}} & \text{if} \quad \|\vec{\mathbf{f}}\|_2 > \frac{v}{2}, \\ \\ 0 & \text{otherwise}. \end{cases} \tag{4.3}$$

The convergence of Algorithm 1 to the minimizer of $\mathcal{J}^{(p)}_{\theta,\omega,\rho}$ can be proved as in [10].

Theorem 4.1. *Let $p = 1, 2, \infty$, and assume*

$$\inf_{\lambda \in \mathbf{\Lambda}} \theta_\lambda (s_{\min} + \omega_\lambda) > \frac{\kappa_q}{4} \tag{4.4}$$

with $s_{\min} := \min \operatorname{Sp}(T^*T)$. Then for any choice $\vec{\mathbf{j}}^{(0)} \in \ell_2(\mathbf{\Lambda}; \mathbb{R}^3)$ the Algorithm 1 converges strongly to a fixed point $\vec{\mathbf{j}}^* \in \ell_2(\mathbf{\Lambda}; \mathbb{R}^3)$ and the couple

$(\vec{\mathbf{j}}^*, v^*)$ *with*

$$v_\lambda^* = \begin{cases} \rho_\lambda - \frac{1}{2\theta_\lambda}\|\vec{\mathbf{j}}^*\|_p & \text{if } \|\vec{\mathbf{j}}^*\|_p < 2\theta_\lambda\rho_\lambda, \\ 0 & \text{otherwise}, \end{cases} \qquad \lambda \in \mathbf{\Lambda}, \tag{4.5}$$

is the unique minimizer of $\mathcal{J}^{(p)}_{\theta,\rho,\omega}(\vec{\mathbf{j}}, v)$*. Moreover, we have the error estimate*

$$\|\vec{\mathbf{j}}^{(k)} - \vec{\mathbf{j}}^*\|_2 \leq \beta^k \|\vec{\mathbf{j}}^{(0)} - \vec{\mathbf{j}}^*\|_2, \tag{4.6}$$

where $\beta := \sup_{\lambda\in\mathbf{\Lambda}} \frac{4\theta_\lambda(1-s_{\min})}{4\theta_\lambda(1+\omega_\lambda)-\kappa_q} < 1$.

The convergence of Algorithm 2 follows from [12, Prop. 3.4].

Now, we want to focus our attention on the term $T^*T\,\vec{\mathbf{j}}^{(k)}$ which appears in the third line of Algorithm 1. The iterative procedure can be implemented only if this term can be efficiently approximated at each iteration step.

The explicit expression of $T^*T\,\vec{\mathbf{j}}$ is given by (cf. [10])

$$\left(T^*T\vec{\mathbf{j}}\right)_{\lambda,\ell} = \sum_{\mu\in\mathbf{\Lambda}}\sum_{m=1}^{3}\left(\sum_{l=1}^{N}(A_{\ell,l}\psi_\lambda)(A_{m,l}\psi_\mu)\right) j_\mu^m, \qquad \lambda \in \mathbf{\Lambda}, \quad \ell = 1,2,3, \tag{4.7}$$

where the operator $A_{\ell,l} : L_2(V_0;\mathbb{R}) \to \mathbb{R}$ is defined as

$$A_{\ell,l}\, f := \frac{\mu_0}{4\pi}\int_{V_0}\left(\frac{\vec{\mathbf{e}}_z(\vec{\mathbf{q}}_l)\times(\vec{\mathbf{r}}\,' - \vec{\mathbf{q}}_l)}{|\vec{\mathbf{r}}\,' - \vec{\mathbf{q}}_l|^3}\right)_\ell f(\vec{\mathbf{r}}\,')\, d\vec{\mathbf{r}}\,'. \tag{4.8}$$

Let $\mathcal{M}$ be the matrix whose entries are the coordinates of T^*T in the multiscale basis $\{\psi_\lambda\}$, i.e.

$$\mathcal{M}_{(\lambda,\ell),(\mu,m)} := \sum_{l=1}^{N}(A_{\ell,l}\psi_\lambda)(A_{m,l}\psi_\mu), \qquad \lambda,\mu \in \mathbf{\Lambda}, \quad \ell,m = 1,2,3. \tag{4.9}$$

From (4.7) it follows

$$\left(T^*T\,\vec{\mathbf{j}}\right)_{\lambda,\ell} = \sum_{\mu\in\mathbf{\Lambda}}\sum_{m=1}^{3} j_\mu^m\, \mathcal{M}_{(\lambda,\ell),(\mu,m)}, \qquad \lambda \in \mathbf{\Lambda}, \quad \ell = 1,2,3. \tag{4.10}$$

Since $\mathcal{M}$ is a bi-infinite matrix, in order to implement an efficient procedure to compute $T^*T\,\vec{\mathbf{j}}^{(k)}$ we need the amplitude of the entries of $\mathcal{M}$ to decay as fast as λ and μ increase.

Let us choose as multiscale basis a compactly supported wavelet basis with $\Omega_\lambda := \mathrm{supp}\,(\psi_\lambda) \sim 2^{-|\lambda|}$, where $|\lambda|$ denote the spatial resolution scale of ψ_λ. Moreover, we assume that the basis functions have d^* vanishing moments, a prescribed smoothness, and fast decay, i.e. $|\psi_\lambda| \le C2^{3/2|\lambda|}$.

It can be shown that $\mathcal{M}$ has compressibility properties w.r.t. such a basis (cf. [10], [18]), so that $T^*T\,\vec{\mathbf{j}}^{(k)}$ can be evaluated with an efficient procedure. In particular, we have

$$
\begin{aligned}
|\mathcal{M}_{(\lambda,\ell),(\mu,m)}| \;\le\; & C2^{-(|\lambda|+|\mu|)(3/2+d^*+1)} \times \\
& \times \begin{cases} N\,\mathrm{dist}(\Omega_\lambda,\Omega_\mu)^{-(3+d^*)} & \text{if } \mathrm{dist}(\Omega_\lambda,\Omega_\mu) > 0, \\ \displaystyle\sum_{l=1}^{N} (\mathrm{dist}(x_l,\Omega_\lambda)\,\mathrm{dist}(x_l,\Omega_\mu))^{-(3+d^*)} & \text{otherwise.} \end{cases}
\end{aligned}
\tag{4.11}
$$

5 A bidimensional test problem

We consider a bidimensional test problem and we assume the current is confined on an horizontal plane S_0, i.e.

$$
\vec{\mathbf{J}}(\vec{\mathbf{r}}) = \big(J_1(x,y), J_2(x,y), 0\big), \qquad (x,y) \in S_0. \tag{5.1}
$$

By substituting (5.1) in (2.6) and integrating over z' we obtain

$$
\mathcal{B}(\vec{\mathbf{J}}, \vec{\mathbf{q}}_l) := \frac{\mu_0}{4\pi} d \int_{S_0} \frac{J_2(x',y')(x'-x_l) - J_1(x',y')(y'-y_l)}{\big((x'-x_l)^2 + (y'-y_l)^2 + z_l^2\big)^{3/2}} dx'\,dy'. \tag{5.2}
$$

Since the current coordinates in the multiscale basis are bidimensional too, i.e.

$$
\vec{\mathbf{j}}_\lambda = (j_\lambda^1, j_\lambda^2, 0), \qquad \lambda \in \mathbf{\Lambda}, \tag{5.3}
$$

the entries of $T^*T\,\vec{\mathbf{j}}$ become

$$
\Big(T^*T\vec{\mathbf{j}}\Big)_{\lambda,\ell} = \sum_{\mu\in\mathbf{\Lambda}} \sum_{m=1}^{2} \left(\sum_{l=1}^{N} (A_{\ell,l}\psi_\lambda)(A_{m,l}\psi_\mu) \right) j_\mu^m, \qquad \lambda \in \mathbf{\Lambda}, \quad \ell = 1,2, \tag{5.4}
$$

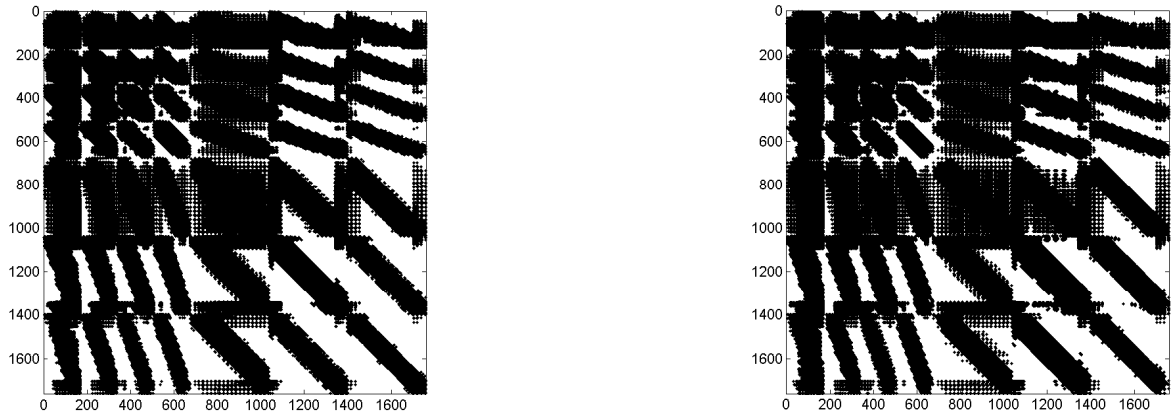

Figure 2: The distribution of the entries of the matrices $T_1T_1^*$ (left) and $T_1T_2^*$ (right). Just the entries that exceed 0.5 are retained.

with

$$A_{1,l}\, f := \frac{\mu_0}{4\pi}\int_{S_0} \frac{-(y\,' - y_l)}{|\vec{\mathbf{r}}\,' - \vec{\mathbf{q}}_l|^3}\, f(\vec{\mathbf{r}}\,')\, d\vec{\mathbf{r}}\,', \quad A_{2,l}\, f := \frac{\mu_0}{4\pi}\int_{S_0} \frac{(x\,' - x_l)}{|\vec{\mathbf{r}}\,' - \vec{\mathbf{q}}_l|^3}\, f(\vec{\mathbf{r}}\,')\, d\vec{\mathbf{r}}\,'. \tag{5.5}$$

We assume there are $N = 400$ sensors located on a regular horizontal grid at a fixed height $\pi = 1\, mm$. In the numerical tests the measured magnetic field is generated by a square current loop of length $1\, cm$ located on S_0.

We choose as a basis the Daubechies orthonormal wavelets with $d^* = 4$ vanishing moments and discretize the plane S_0 with 32 pixels for each dimension. Finally, 2 multiresolution levels are used for the current decomposition.

We have realized a MATLAB code running on a Personal Computer. It takes about 20 *min* for the construction of the matrix $\mathcal{M}$ and about 83 *sec* for 100 iterations of the algorithm.

In Fig. 2 the distribution of the entries of the matrices $T_1T_1^*$ and $T_1T_2^*$ with amplitude greater than $10^{-4}(\|\mathcal{M}\|_\infty/\dim \mathcal{M}) \approx 0.5$ are displayed. Just about 25% of the entries are retained. The matrices $T_2T_1^*$ and $T_2T_2^*$ have a similar behaviour.

In Fig. 3 the measured magnetic field is displayed (the sensor locations are displayed as black points). In Fig. 4 the current distribution reconstructed

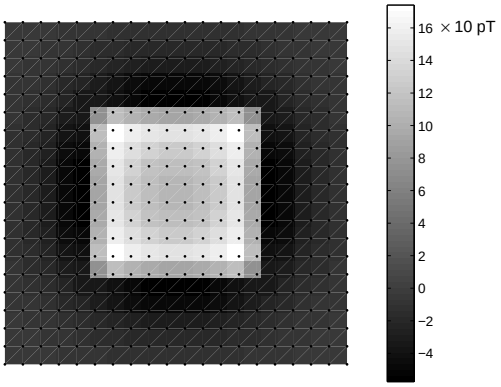

Figure 3: The magnetic field (pT) produced by a square current loop (black line) and the magnetometer distribution (black points).

after 120 iterations of the proposed algorithm is shown. Actually, in this case the inverse problem is well-posed [2] and can be solved without a regularization procedure: indeed, the Tikhonov regularization with regularization parameter set equal to 0 gives a similar result.

In Fig. 6 the current distribution reconstructed after 30 iterations of Algorithm 1 is displayed when high white Gaussian noise with linear signal to noise ratio 1 is added to the magnetic field of Fig. 5. The thresholding parameter $\{\rho_\lambda\}_{\lambda\in\mathbf{\Lambda}}$ is chosen as

$$\rho_{|\lambda|} = \sigma\sqrt{\frac{2\log(2^{|\lambda|}N)}{2^{|\lambda|}N}},$$

where σ is the noise level and $|\lambda| = 0, 1, 2$, is the multiresolution level scale (cf. [7]). In the example $\sigma \approx 133\,pT$, $\rho_0 \approx 15\,pT$; $\{\omega_\lambda\}_{\lambda\in\mathbf{\Lambda}} = 0$, $\{\theta_\lambda\}_{\lambda\in\mathbf{\Lambda}} = 1$.

In case of measurements with high noise, Tikhonov regularization is not able to give an accurate current image: when the regularization parameter is chosen equal to 0 the current is not reconstructed at all (see Fig. 7, left), while a regularization parameter greater than 0 gives a blurred image (see Fig. 7, right, where the regularization parameter is chosen by means of the discrepancy principle and is equal to 356).

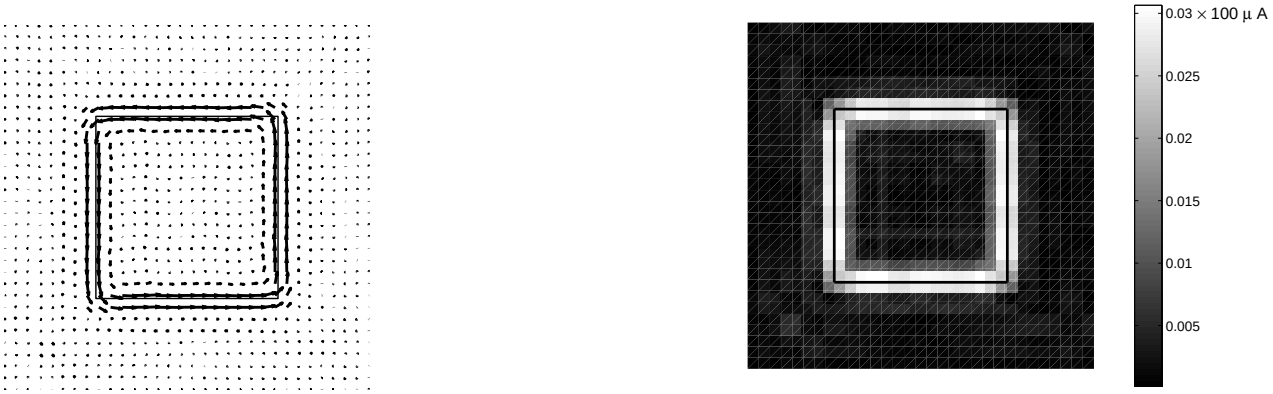

Figure 4: The current distribution (left) reconstructed starting from the magnetic field displayed in Fig. 3. The current intensity (μA) is also displayed (right). The black square represents the current loop.

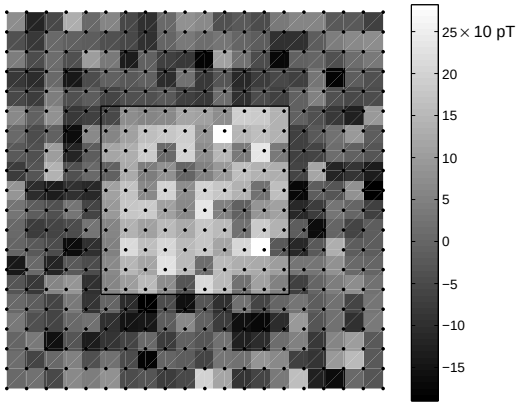

Figure 5: The noisy magnetic field (pT) produced by a square current loop (black line) and the magnetometer distribution (black points).

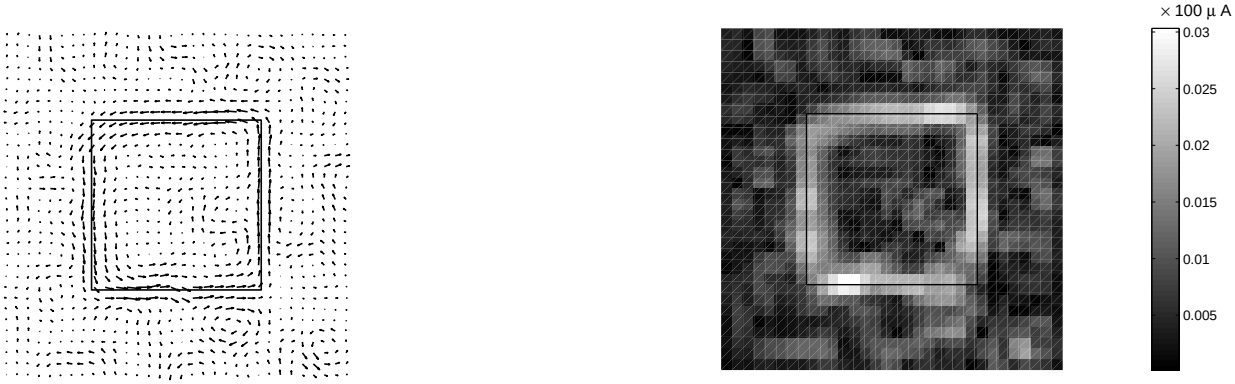

Figure 6: The current distribution (left) reconstructed starting from the noisy magnetic field displayed in Fig. 5. The current intensity (μA) is also displayed (right). The black square represents the current loop.

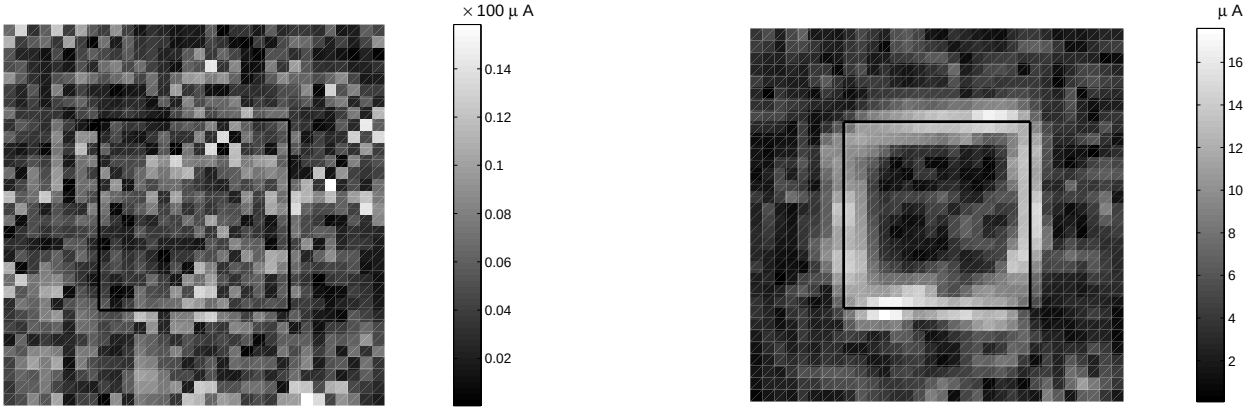

Figure 7: The current distribution reconstructed by using the Tikhonov regularization starting from the noisy magnetic field displayed in Fig. 5. Two different values of the regularization parameter have been used: 0 (right) and 356 (right). The black square represents the current loop.

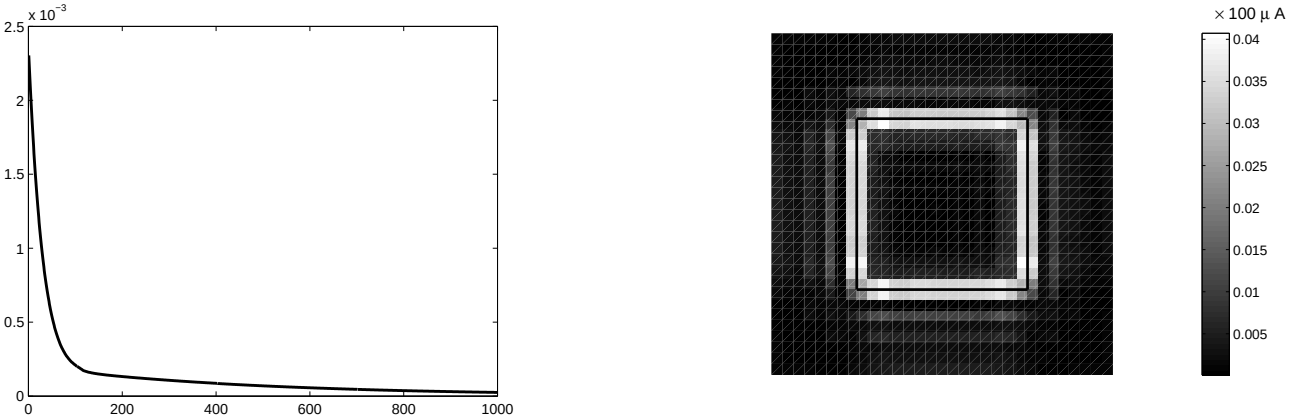

Figure 8: The norm of the difference between two successive iterations for the first 1000 iterations of the proposed algorithm (left). The reconstructed current density is also displayed (right). The plot refers to the magnetic field measurements displayed in Fig. 4.

6 Conclusion

The numerical tests in Section 6 show that the proposed algorithm outperforms Tikhonov regularization in the case when the magnetic field is affected by high noise. This behaviour would be more evident in the three-dimensional case, where the problem is highly ill-posed and ill-conditioned, and we expect our algorithm to give better results than the usual Tikhonov regularization.

In order to implement efficiently Algorithm 1 in the three-dimensional case we need to solve some practical problems. First of all, the dimension of the matrix approximating $\mathcal{M}$ dramatically increases and, moreover, accurate results require a high resolution, i.e. a high pixel number. This means that we have to improve compressibility properties of $\mathcal{M}$ by using a different, and better suited, multiscale basis.

Secondly, the convergence rate of the proposed algorithm can be very slow (see Fig. 8) and acceleration techniques are mandatory. At present acceleration techniques have been proposed in the scalar case [9], [16]. An extension to the three-dimensional case will be the subject of further investigations.

References

[1] M. Bertero, P. Boccacci, *Introduction to inverse problems in imaging*, Institute of Physics, Bristol, Philadelphia, 2002.

[2] J.R. Bradley, J.P. Wikswo, N.G. Sepulveda, Using a magnetometer to image a two-dimensional current distribution, J. App. phys. 65 (1989), 361–372.

[3] O. Christensen, *An Introduction to Frames and Riesz Bases*, Birkhäuser, 2003.

[4] I. Daubechies, *Ten Lectures on Wavelets*, SIAM, 1992.

[5] I. Daubechies, M. Defrise and C. De Mol, An iterative thresholding algorithm for linear inverse problems with a sparsity constraint, *Commun. Pure Appl. Math* 57 (2004), 1413–1457.

[6] D.L. Donoho, Superresolution via Sparsity Constraints, SIAM J. Math. Anal. 23 (1992), 1309–1331.

[7] D.L. Donoho, De-noising by soft-thresholding, IEEE Trans. Inform. Theory 41 (1995), 613–627.

[8] H.W. Engl, M. Hanke and A. Neubauer, *Regularization of inverse problems*, Kluwer, Dordrecht, 2000.

[9] I. Daubechies, M. Fornasier, I. Loris, Accelerated projected gradient methods for linear inverse problems with sparsity constraints, J. Fourier Anal. Appl., to appear, 2008.

[10] M. Fornasier, F. Pitolli, Adaptive iterative thresholding algorithms for magnetoencephalography (MEG), J. Comput. Appl. Math. 221 (2008), 386–395.

[11] M. Fornasier, H. Rauhut, Recovery algorithms for vector-valued data with joint sparsity constraints, SIAM J. Numer. Anal. 46 (2008), 577–613.

[12] M. Fornasier, H. Rauhut, Iterative thresholding algorithms, Appl. Comput. Harmon. Anal. 25 (2008), 187–208.

[13] J.D. Jackson, *Classical Electrodynamics*, John Wiley & Sons, Inc., 1975.

[14] J. Kaipio, E. Somersalo, *Statistical and computational inverse problems*, Applied mathematical sciences 160, Springer, New York, 2005.

[15] R. Kress, L. Kühn, R. Potthast, Reconstruction of a current distribution from its magnetic field, Inverse Problem 18 (2002), 1127–1146.

[16] R. Ramlau, G. Teschke, M. Zhariy, A compressive Landweber iteration for solving ill-posed inverse problems, Inverse Problems, to appear, 2008.

[17] J. Sarvas, Basic mathematical and electromagnetic concepts of the biomagnetic inverse problem, Phys. Med. Biol. 32 (1987), 11–22.

[18] R. Schneider, Multiskalen- und Wavelet-Matrixkompression: Analysisbasierte Methoden zur effizienten Lösung grosser vollbesetzter Gleichungssysteme, Advances in Numerical Mathematics, Teubner Stuttgart, 1998.

[19] J.P. Wikswo, Applications of SQUID magnetometers to biomagnetism and nondestructive evaluation, in *Applications of Superconductivity* (H. Weinstock ed.), Kluwer Academic Publishers, Netherlands, 2000, 139–228.